applied sciences

MDPI

Article

Study on Nonlinear Aerodynamic Characteristics of a Semi-Closed Box Bridge Deck Based on Coupled Amplitude Variation

Haoyang Lu, Jie Jia *, Lixin Zhang and Lin Dong

School of Civil Engineering, Northeast Forestry University, Harbin 150040, China; luhaoyangcontrol@126.com (H.L.); zhanglix1998@163.com (L.Z.); 13154566987@163.com (L.D.)
* Correspondence: jiajiecontrol@126.com

Abstract: This paper explores the nonlinear characteristics of the self-excited aerodynamic forces of a semi-closed box deck section to perfect the theory of aeroelastic response analysis. A numerical wind tunnel model was established based on the computational fluid dynamics (CFD) method. The heaving-pitching coupled motion is realized by loading user-defined function (UDF) and dynamic grid technology. The self-excited aerodynamic forces varying with amplitude are identified and analyzed, and the reliability of the aerodynamic results obtained by numerical simulation is verified in the wind tunnel test. In the heaving-pitching coupled motion, the results show that the nonlinear characteristics of aerodynamic forces, especially the aerodynamic moment, are mainly affected by the pitching motion. The phenomenon of high-order harmonic energy transfer is observed with the increase in pitching amplitude, and the main component of high-order harmonic can be determined by the pitching amplitude. The contribution of heaving motion to aerodynamic forces nonlinear components is small, but its influence on nonlinear characteristics is complex. Small amplitude heaving motion plays a positive damping role in heaving-pitching coupled motion, and its scope and effect of positive damping action are affected by pitching motion. The extreme value heaving amplitude of positive damping action is observed in the aerodynamic lift.

Keywords: long-span bridge; nonlinear self-excited aerodynamic force; flutter; limit cycle oscillations (LCO); computational fluid dynamics (CFD)

Citation: Lu, H.; Jia, J.; Zhang, L.; Dong, L. Study on Nonlinear Aerodynamic Characteristics of a Semi-Closed Box Bridge Deck Based on Coupled Amplitude Variation. *Appl. Sci.* **2022**, *12*, 7609. https://doi.org/10.3390/app12157609

Academic Editor: Jong Wan Hu

Received: 6 July 2022
Accepted: 26 July 2022
Published: 28 July 2022

1. Introduction

With the continuous progress of engineering research and technology, bridge spans are increasing and have broken through 2000 m class, which makes bridges more sensitive to wind and may cause more severe vibration of the main beam [1]. Flutter belongs to large amplitude self-excited vibration, which can cause catastrophic damage. The self-excited vibration is related to the self-excited aerodynamic forces acting on the main beam, and the self-excited aerodynamic forces are related to the structure shape [2,3] and its motion form [4–6]. Therefore, the aerodynamic system of the bridge deck with an apparent blunt body shape may have significant nonlinear characteristics under large amplitude motion. At this time, the nonlinear effect of self-excited aerodynamic forces cannot be ignored.

The linear self-excited forces model proposed by Scanlan [7] is utilized as the basis of the current flutter calculation theory, which is based on the assumption of minor disturbance and small amplitude. In fact, due to the influence of aerodynamic forces nonlinearity and structural nonlinearity, the post-flutter behavior of bridge deck may not be divergent vibration, but enter a limit cycle oscillations (LCO) state of stable amplitude. This nonlinear flutter phenomenon, also known as soft flutter, has been found by many scholars in tests [8–15]. Daito et al. [3] observed the obvious LCO when studying the aerodynamic characteristics of two-edge girders, and considered that the geometric shapes sensitively affect the flutter stability. When studying the aerodynamic response of a rigid flat and

rectangular steel plate of chord length and thickness ratio 1:23.3, LCO under coupled-mode flutter was discovered in the wind tunnel by Amandolese et al. [12], which appeared below the critical flutter velocity. The flutter performance test of streamlined box deck section under a large amplitude was carried out by Xu et al. [16], and the opposite law was found in the variation in heaving and pitching amplitude ratio of coupled LCO and divergent vibration with amplitude. With the development of computer technology and CFD, numerical simulation, as a cost-effective method, is widely used in the study of nonlinear aerodynamic forces [17–20]. Mannii et al. [2] investigated the amplitude dependence of self-excited aerodynamic forces in small amplitude motion state, and the results showed that the flutter derivative was more sensitive to the motion amplitude in the sharp-edge configuration. Zhang et al. [21] also performed amplitude dependence studies through two-dimensional numerical simulation. They identified that the pitching amplitude of 10° can be used as the critical value to distinguish the flow pattern of the flow field around the section. Jia et al. [22] investigated the characteristics of nonlinear aerodynamic forces varying with amplitude, frequency and the angle of attack under single degree of freedom motion. They found that the effect of amplitude on the nonlinear components of pitching motion is generally higher than that of heaving motion. The energy budget analysis of the post-flutter LCO was carried out by Zhang et al. [23], using the CFD numerical simulation method. The results show that the higher-order components of the self-excited forces contribute insignificantly in the energy input for the post-flutter LCO of the streamlined box deck. Most of the above analyses of nonlinear self-excited aerodynamic forces involve two issues. Firstly, the current research on nonlinear self-excited aerodynamic forces mainly focuses on flat plate or streamlined box bridge decks, but their nonlinear characteristics are not significant compared with the severely blunted bridge decks. Secondly, the nonlinear characteristics of self-excited aerodynamic forces in heaving motion are weak, and the heaving amplitude range selected in relevant studies is not large enough. Therefore, the relationship between nonlinear aerodynamic forces and forced large amplitude (especially heaving amplitude) is not clear enough. The semi-closed box deck is the research object of this paper. It has many advantages, such as lower cost, less difficulty in construction and more convenient maintenance. The semi-closed box deck section has more obvious LCO phenomenon, which was put forward by Zhu et al. [24,25] when researching four kinds of typical sections. The significant aerodynamic nonlinear effect leads to more complex wind-resistant stability problems, which makes the theory of linear flutter analysis inconsistent with the actual situation. In this paper, the dynamic grid technique with UDF loading is used to control the amplitude of section motion to realize the numerical simulation of pitching-heaving coupled forced vibration. In order to reveal the nonlinear characteristics of self-excited aerodynamic forces under different coupling amplitudes, the time domain and frequency domain signals are analyzed to clarify the importance and variation law of each high-order harmonic component under different amplitude combinations. The research on nonlinear aerodynamic characteristics of bridges under large vibration amplitude is beneficial to deeply understand the nonlinear effects of self-excited aerodynamic forces, and build a nonlinear flutter theoretical framework, which lays a foundation for the establishment of nonlinear self-excited aerodynamic models with broad applicability and higher accuracy. In addition, it can help to reasonably estimate the flutter critical wind speed and post flutter behavior of bridges, so as to obtain the ability to predict the flutter amplitude response, and provide reference and support for the design and analysis of bridges with an extra-large span.

2. Numerical Simulation of Forced Vibration

2.1. Turbulence Modelling

An excellent turbulence model can reduce the amount of numerical calculation and ensure the accuracy of the results. In the rectangular coordinate system, the N-S equation of viscous incompressible fluid after Reynolds averaging (RANS) is:

$$\frac{\partial(\rho\overline{u}_i)}{\partial t} + \frac{\partial(\rho\overline{u}_j\overline{u}_i)}{\partial x_j} = -\frac{\partial\overline{p}}{\partial x_i} + \mu\frac{\partial}{\partial x_j}\left(\frac{\partial\overline{u}_i}{\partial x_j} - \rho\overline{u_i'u_j'}\right) \tag{1}$$

where $\overline{u}_i$ and $\overline{u}_j$ are the average velocity component; u_i' and u_j' are the pulsating velocity component; t is the time; ρ = 1.225 kg/m^3 is the air density; $\overline{p}$ is the average pressure; $\mu = 1.7894 \times 10^{-5}$ kg/m·s is the dynamic viscosity coefficient.

The new unknown quantity $\rho\overline{u_i'u_j'}$ is generated by averaging the operation, so the key to making the equations closed is to introduce a model to solve it. The following assumptions are included in the eddy viscosity model proposed by Boussinesq [26]:

$$-\rho\overline{u_i'u_j'} = \mu_i\left(\frac{\partial\overline{u_i}}{\partial x_j} + \frac{\partial\overline{u}_j}{\partial x_i}\right) - \frac{2}{3}\rho k\delta_{ij} \tag{2}$$

where k is turbulent kinetic energy; μ_i is turbulent viscosity.

According to the different applications of turbulence characteristic quantities in eddy viscosity model, different turbulence models have been proposed by scholars. The commonly used turbulence models can be classified into: zero-equation model, one-equation model and two-equation model according to the number of differential equations used. For general flow, the calculation accuracy is higher and the calculation amount is larger with the number of equations. Common two-equation models include standard k-ε model, RNG k-ε model, standard k-ω model and SST k-ω model, etc.

SST (Shear Stress Transport) k-ω model was proposed by Menter [27] based on k-ε model and k-ω model. It uses the k-ω model for the near-wall grid area and the k-ε model for the grid area further away from the wall. Because the advantages of k-ε model and k-ω model are combined by mixed functions, the SST k-ω model has higher reliability and accuracy, and is widely used. The expression of the SST k-ω model is:

$$\rho\frac{Dk}{Dt} = \frac{\partial}{\partial x_j}\left(\mu_{eff,k}\frac{\partial k}{\partial x_j}\right) + S^k \tag{3}$$

$$\rho\frac{D\omega}{Dt} = \frac{\partial}{\partial x_i}\left(\mu_{eff,\omega}\frac{\partial k}{\partial x_i}\right) + S^\omega \tag{4}$$

where $\mu_{eff,k}$ and $\mu_{eff,\omega}$ is the equivalent viscosity of the turbulent term; S^k and S^ω is the source term of the specific dissipation rate of turbulent kinetic energy.

The reliability of numerical results using the SST k-ω model has been confirmed by many scholars [28–31]. In view of this, the SST k-ω model is used to model the turbulence viscosity in this paper. The incoming flow has been set at a turbulence intensity of 0.5%, and the ratio of turbulence viscosity to molecular viscosity is 2.

2.2. Sectional Model and Computational Domain

All discussions in this paper are conducted by taking the semi-closed box deck section of the Second Jiaojiang Bridge (see Figure 1) in Taizhou, Zhejiang Province, China as a background. The scale ratio of the deck section model to actual bridge was set as 1:80, the cross section of the sectional model is shown as Figure 1. The width (B) and depth (D) of the model were, respectively, about 0.532 m and 0.044 m, and the width to depth ratio is 12.17.

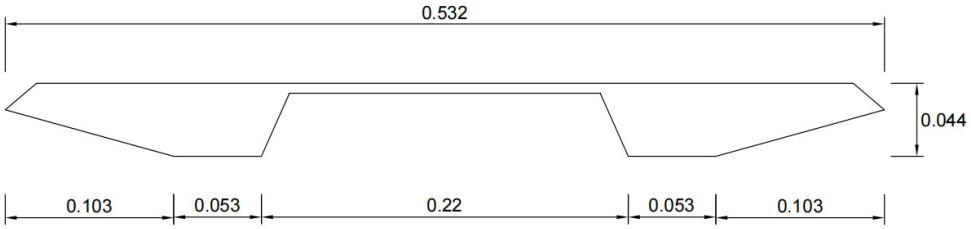

Figure 1. Deck section dimensions and shape (m).

The two-dimensional grid is used in the nonlinear aerodynamic simulation under the heaving-pitching coupled motion, and its reliability has been verified by many scholars [2,20–23]. The two-dimensional rectangular computational domain is shown in Figure 2. The left boundary is set as the velocity inlet, which is 5*B* (i.e., 61*D*) away from the front end of the sectional model. The right boundary is set as the pressure outlet, which is 13*B* (i.e., 158*D*) away from the end of the sectional model, and the reference pressure is zero. Both the upper and the lower boundaries are defined as symmetrical boundary conditions, and the distance from the center of the sectional model is 4*B* (i.e., 49*D*). Both the upper and the lower boundaries are defined as symmetry, and the distance from the center of the sectional model is 4*B* (49*D*). The largest blocking ratio during vibration is 4.3%.

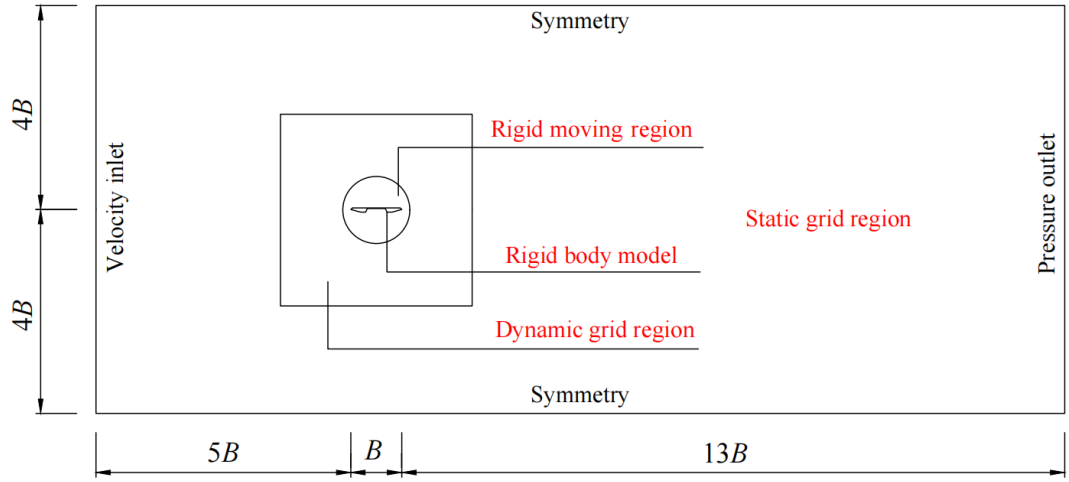

Figure 2. Schematic diagram of model computing domain.

2.3. Dynamic Grid Technology

The grid division method of "rigid moving region + dynamic grid region + static grid region" is adopted to ensure the high quality of the near wall grid when the sectional model is moving. The rigid moving region and the static grid region consist of structured quadrilateral grids, and the dynamic grid region is composed of unstructured triangular grids, as shown in Figure 3. After independent verification of grid number and time step by Jia et al. [22], the final grid number is determined to be 505,334, and the time step is selected to be 0.0001 s. Local details of the grid around the section are shown in Figure 4. According to the requirements of the SST *k*-ω turbulence model for the near wall grid, the y^+ value is taken as 1 [32]. The height of the first-layer grid near the wall surface is calculated as $\Delta y = 6 \times 10^{-5}$ m by Equation (5), and the normal growth rate is set as 1.01.

$$\Delta y = \frac{\mu Y^+}{\rho u_\tau} \tag{5}$$

where $u_\tau = \sqrt{\frac{\tau_\omega}{\rho}}$ is the wall friction velocity; τ_ω is the wall shear stress; $\frac{\mu}{\rho}$ is the kinematic viscosity coefficient.

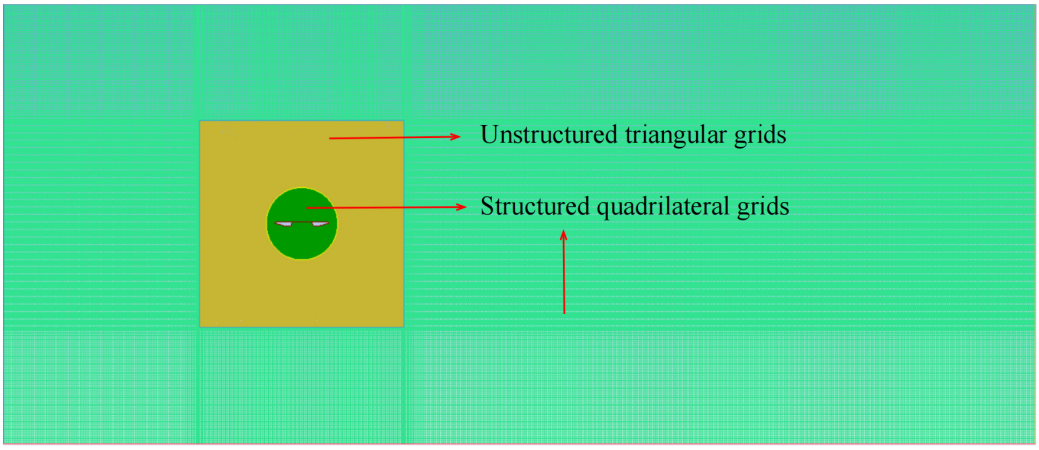

Figure 3. Grid of the whole computational domain.

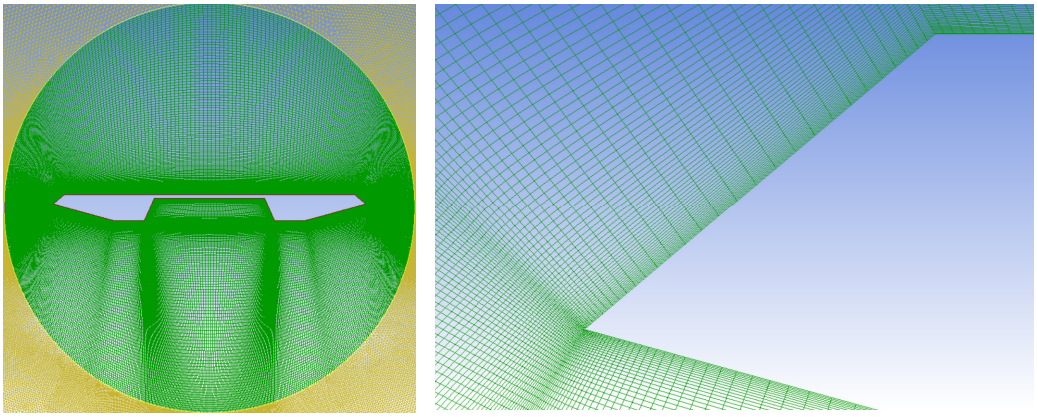

Figure 4. Grid of Local details. (**a**) Rigid moving region (**b**) Front edge near wall.

The pitching and heaving motions are combined (see Figure 5), and they are simple harmonic vibrations with the same frequency. Point E is the shear center, located 0.393D from the top of the sectional model, and it is also the center of motion. The lift force $L(t)$ and the moment $M(t)$ at the center of plate, defined in Figure 5. The corresponding lift and moment coefficients are defined as:

$$C_L = \frac{L(t)}{0.5\rho U^2 B} \tag{6}$$

$$C_M = \frac{M(t)}{0.5\rho U^2 B^2} \tag{7}$$

where ρ is the air density, U is the speed of uniform inflow, and B is the width of deck section.

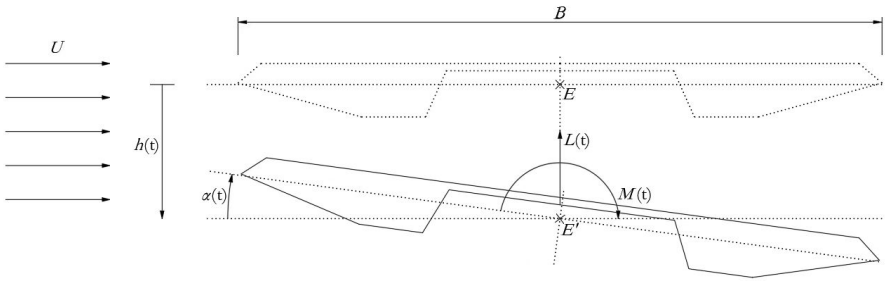

Figure 5. Schematic diagram of the pitching and heaving combined motion of the sectional model.

Forced vibration is realized by loading UDF, and the grid update of forced vibration is implemented by assigning the motion form to the DEFINE_CG_MOTION macro. Two dynamic grid updating methods, smoothing and remeshing, are combined to ensure the efficiency and quality of grid updating. The motion expression of coupled motion is calculated as:

$$h(t) = h_0 \sin(2\pi f t) \tag{8}$$

$$\alpha(t) = \alpha_0 \sin(2\pi f t) \tag{9}$$

where h_0 and α_0 are the heaving forced amplitude and pitching forced amplitude, respectively; f is the forced frequency.

A second-order implicit scheme and a second-order upwind scheme are adopted to solve the pressure and momentum equations, respectively. The decoupling of pressure and velocity is treated by SIMPLEC algorithm.

2.4. Reliability Verification

The semi-closed box deck of the Second Jiaojiang Bridge lacks aerodynamic data to verify grid reliability. Therefore, in this paper, the aerodynamic forces data are measured by wind tunnel test, and compared with the aerodynamic forces results obtained by numerical simulation. The wind tunnel test was conducted in the second test section of the wind tunnel (see Figure 6), a closed-circuit wind tunnel located in the Northeast Forestry University, China.

Figure 6. Partial view of wind tunnel.

The test section has width and height of 0.8 m and 1 m, respectively. The wind speed can be adjusted from 5 m/s to 70.5 m/s. The quality of the flow field is very stable. The flow is nearly laminar with a uniform velocity profile at the inlet, and the turbulence intensity of the empty wind tunnel is less than 0.5% on average.

The scale ratio between section model and actual bridge is 1:80, which is consistent with the section size in the numerical wind tunnel. The model has a streamwise width, B, of 0.532 m, a height, D, of 0.044 m, and a span, L, of 0.82 m. The blockage ratio of the model at 0° wind attack angle is 4.5%, which meets the requirements of wind tunnel test that the blocking rate is less than 5%. Two identical end plates (0.72 m wide and 0.12 m high) are installed on both sides of the section model to prevent end effect and enable a close to bi-dimensional flow field. The section model placed in the wind tunnel is shown in Figure 7. The static forces test is completed by a six-component balance, as shown in Figure 8. The section model is rigidly connected with the force measuring balance. The balance is placed on a rigid base that can adjust the height, and the two are also rigidly connected. The bottom of the model is raised a sufficient distance from the wind tunnel wall to ensure uniform flow field, avoiding the influence of wind speed profile as far as possible.

Figure 7. Test model in wind tunnel.

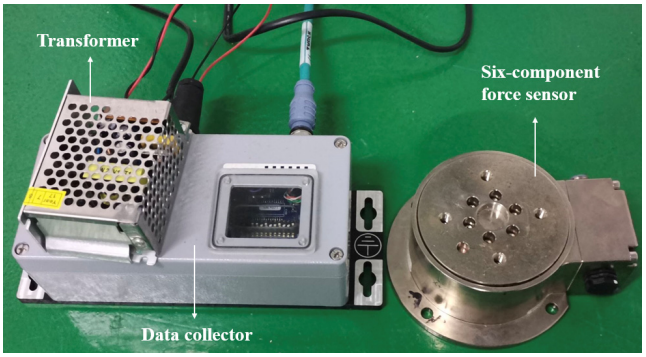

Figure 8. Six-component balance.

Three groups of tests for measuring aerodynamic coefficients of semi closed box girder sections were carried out to prevent accidental errors. The sampling time of each group is set to 60 s and the sampling frequency is set to 1000 Hz. The average of three experimental results is taken as a final result, as shown in Table 1. The errors of drag coefficient and lift coefficient are about 5%, proving the reliability of the numerical simulation grid in this paper.

Table 1. Verification of grid reliability.

	Drag Coefficient	Lift Coefficient
Numerical simulation	0.424	−0.262
Wind tunnel test	0.449	−0.248

3. Results and Discussion

To explore the characteristics of aerodynamic nonlinear components under different combination amplitudes, the following work was carried out at zero angle of attack, a forced frequency of 4 Hz and uniform wind speed of 12.8 m/s. The reduced wind speeds can be calculated as:

$$U^* = \frac{U}{fB} \tag{10}$$

where U is uniform wind speed, f is the forced frequency, and B = 0.532 m is the width of deck section.

The selected cases about different amplitudes are listed in Table 2.

Table 2. Operation setting.

Figure	Reduced Velocity	Heaving Amplitude	Pitching Amplitude
4	6	0.02*B*	2°
		0.04*B*	4°
		0.08*B*	8°
		0.1*B*	10°
		0.16*B*	16°
		0.2*B*	20°

3.1. Amplitude Dependence of High-Order Harmonic Components in Heaving-Pitching Coupled Motion

The aerodynamic time-domain data are identified through numerical simulation, and the aerodynamic time history curves of five stable periods are taken as shown in Figure 9. As can be seen from Figure 9a, slight waveform distortion can be observed in the aerodynamic time history curve under heaving-pitching coupled motion with small amplitude, and the harmonic characteristics of aerodynamic lift are worse than that of aerodynamic moment. This indicates that the high-order harmonic components have begun to emerge in the case of small amplitude. After increasing the combined amplitude, severe waveform distortion can be observed in both aerodynamic lift and moment, as reported in Figure 9b. That is to say, with the increase in amplitude, the content of high-order harmonic components increases, which makes the harmonic characteristics of time history curve destroyed obviously.

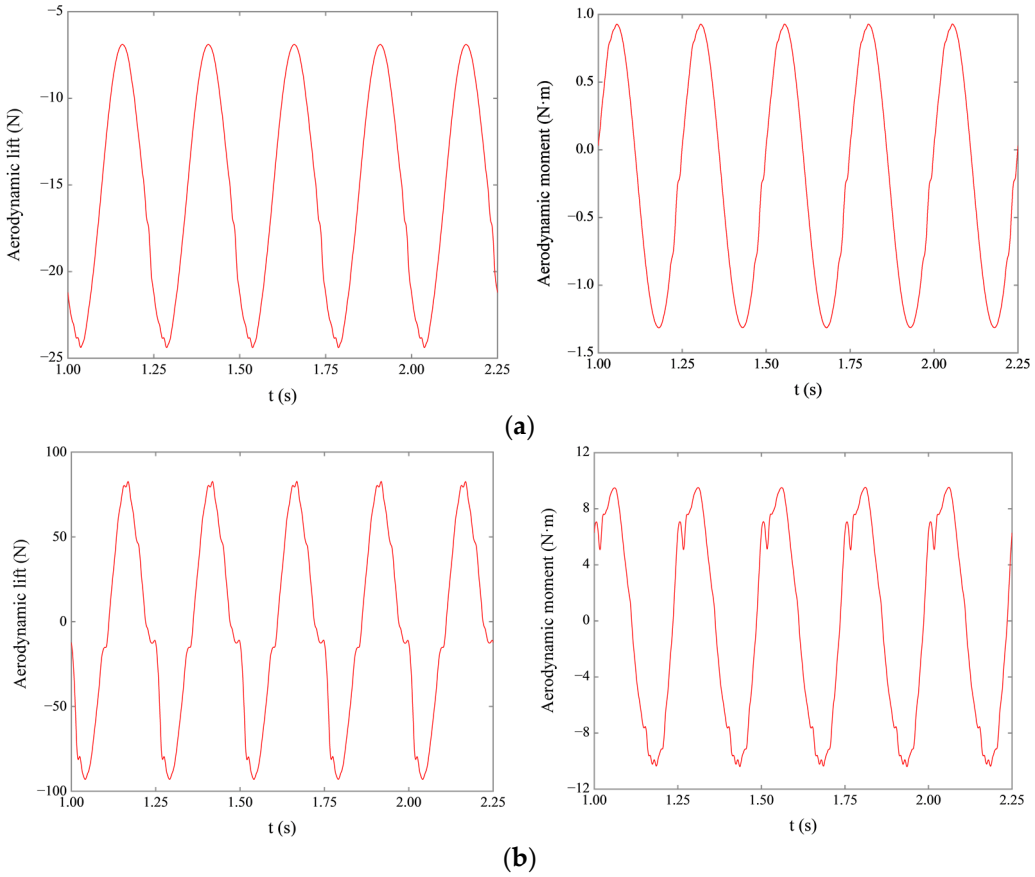

Figure 9. Time history curve of aerodynamic forces. (**a**) Small amplitude motion ($\alpha_0 = 2°$, $h_0 = 0.02B$). (**b**) Large amplitude motion ($\alpha_0 = 20°$, $h_0 = 0.2B$).

In order to deeply explore the variation law of nonlinear aerodynamic components under different combined amplitudes, ten stable periods of time history curve are taken to

obtain the frequency domain data by fast Fourier transform (FFT), and the nonlinear components of aerodynamic forces represented by the second to fifth harmonics are analyzed.

Heaving motions with different amplitudes (h_0 = 0.02B, 0.04B, 0.08B, 0.1B, 0.16B, 0.2B) are added to three groups of foundation pitching motions (α_0 = 2°, 8°, 16°), and the spectrum diagram is shown in Figures 10 and 11. The high-order harmonic components of the aerodynamic forces are increased with the added heaving amplitude, and the high-order harmonic main components of the aerodynamic lift are transferred from the second harmonic to the third. Moreover, when the foundation pitching amplitude is larger, the heaving amplitude required for the third harmonic to dominate is smaller. The higher harmonic components of aerodynamic moment increase evenly with the amplitude, and the main component is always the second harmonic.

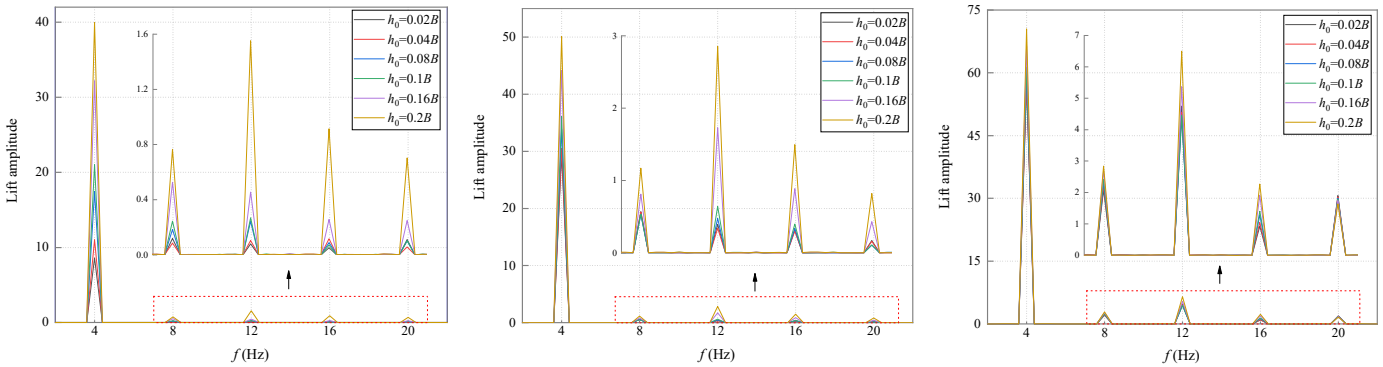

Figure 10. Aerodynamic lift spectrum under different coupled amplitude. (**a**) Pitching amplitude α_0 = 2° (**b**) Pitching amplitude α_0 = 8° (**c**) Pitching amplitude α_0 = 16°.

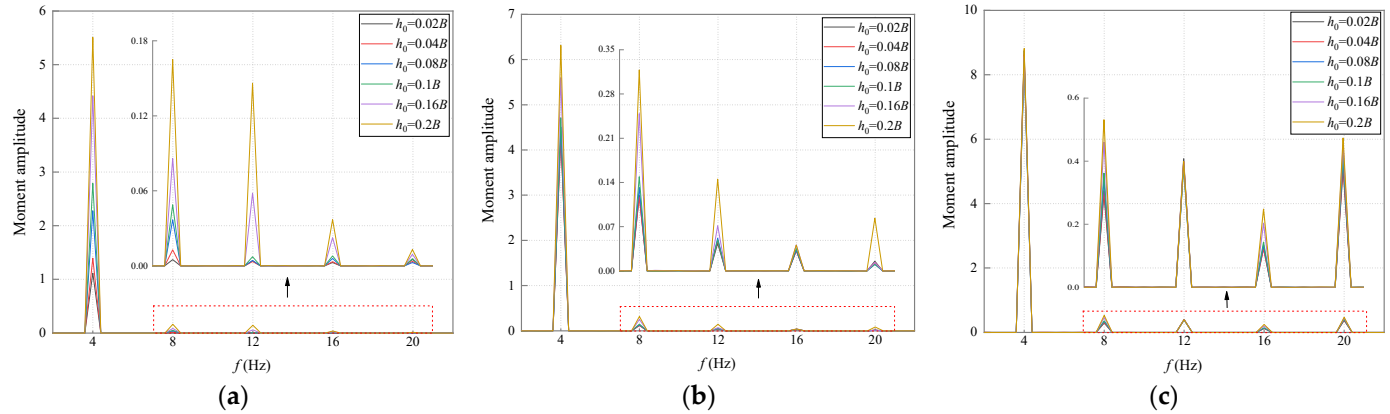

Figure 11. Aerodynamic moment spectrum under different coupled amplitude. (**a**) Pitching amplitude α_0 = 2° (**b**) Pitching amplitude α_0 = 8° (**c**) Pitching amplitude α_0 = 16°.

Pitching motions with different amplitudes (α_0 = 2°, 4°, 8°, 10°, 16°, 20°) are added to three groups of foundation heaving motions (h_0 = 0.02B, 0.1B, 0.2B), and the spectrum diagram is shown in Figures 12 and 13. The main component of the aerodynamic lift and moment is transferred from the second harmonic to the third with the increase in the added pitching amplitude, and the pitching amplitude required for the energy transfer of the aerodynamic lift is smaller than moment. The increase in the foundational heaving amplitude can promote the energy transfer phenomenon of aerodynamic lift, but restrain the harmonic energy transfer of aerodynamic moment.

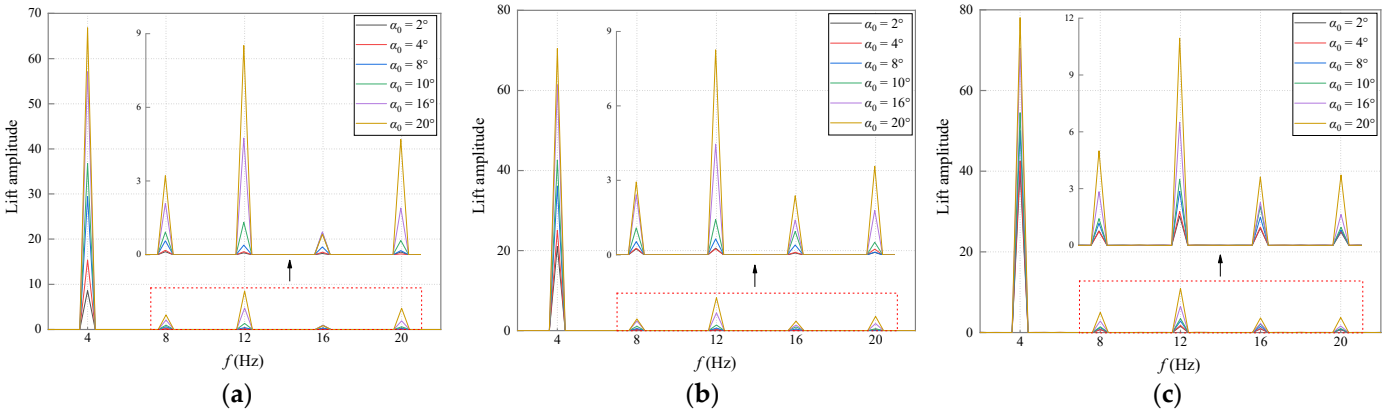

Figure 12. Aerodynamic lift spectrum under different coupled amplitude. (**a**) Heaving amplitude $h_0 = 0.02B$ (**b**) Heaving amplitude $h_0 = 0.1B$ (**c**) Heaving amplitude $h_0 = 0.2B$.

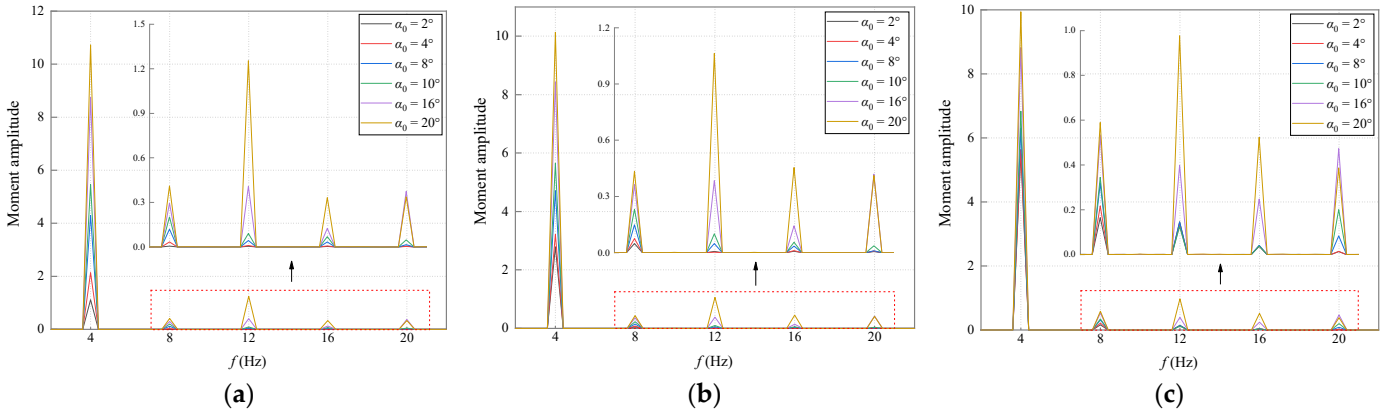

Figure 13. Aerodynamic moment spectrum under different coupled amplitude. (**a**) Heaving amplitude $h_0 = 0.02B$ (**b**) Heaving amplitude $h_0 = 0.1B$ (**c**) Heaving amplitude $h_0 = 0.2B$.

Therefore, in the flutter calculation of the semi-closed box deck section, the importance of the third harmonic component should be given priority in the aerodynamic lift when the pitching amplitude is larger ($\alpha_0 > 10°$). For the aerodynamic moment, heaving and pitching amplitudes should be considered comprehensively to determine the importance of the high-order harmonic component in large amplitude motion. When the pitching amplitude is small ($\alpha_0 < 10°$), the importance of the second harmonic component should be given priority.

3.2. Influence of Bending-Torsional Coupled Effect on Nonlinear Aerodynamics

When the heaving and pitching are combined, one degree of freedom is bound to affect the other, and the interaction between the two motion modes leads to the existence of bending-torsional coupled term in aerodynamic forces. In order to observe the characteristic law of the interaction between the two degrees of freedom in heaving-pitching coupled motion, another motion form with different amplitudes is added to a specific basic motion, and the aerodynamic results are compared with the single degree of freedom (abbreviated as 1-DOF) motion.

The variation in fundamental frequency, the second and third harmonic of aerodynamic lift and moment with heaving motion amplitude is reported in Figures 14 and 15. It can be seen from Figures 14a and 15a that in the state of 1-DOF pitching motion, with the increase in heaving amplitude, the fundamental frequency amplitude of aerodynamic forces has a roughly positive linear relationship with heaving amplitude. The linear relationship is destroyed when the foundational pitching motion exists, and the larger the foundational pitching motion amplitude is, the worse the linear relationship is, and the

slower the growth rate of the fundamental frequency amplitude with heaving amplitude is. As shown in Figure 14b, for the aerodynamic lift, the curve shape of the second and third harmonic with the increase in heaving amplitude can hardly be damaged due to the change in the foundational pitching amplitude. The growth rate of the third harmonic is significantly higher than that of the second harmonic when the heaving amplitude is large (0.1*B*). Therefore, the phenomenon that the main components of high-order harmonic are transferred from the second harmonic to the third harmonic will appear with the increase in the heaving amplitude. As shown in Figure 15b, the curve shape of the second harmonic is basically not affected by the change in the foundational pitching amplitude, but the curve shape of the third harmonic is changed by it. In the heaving-pitching coupled motion, the pitching motion dominates the nonlinear characteristics of aerodynamic lift and moment by affecting the third harmonic, and the promotion of the nonlinear characteristics by the heaving motion is mainly reflected in the aerodynamic lift.

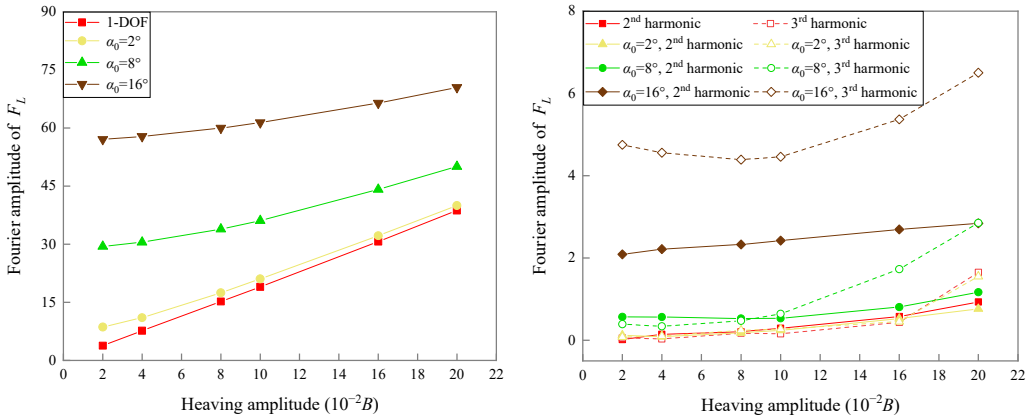

Figure 14. Variation in Fourier amplitude of aerodynamic lift with heaving amplitude. (**a**) The fundamental frequency (**b**) Second harmonic and third harmonic.

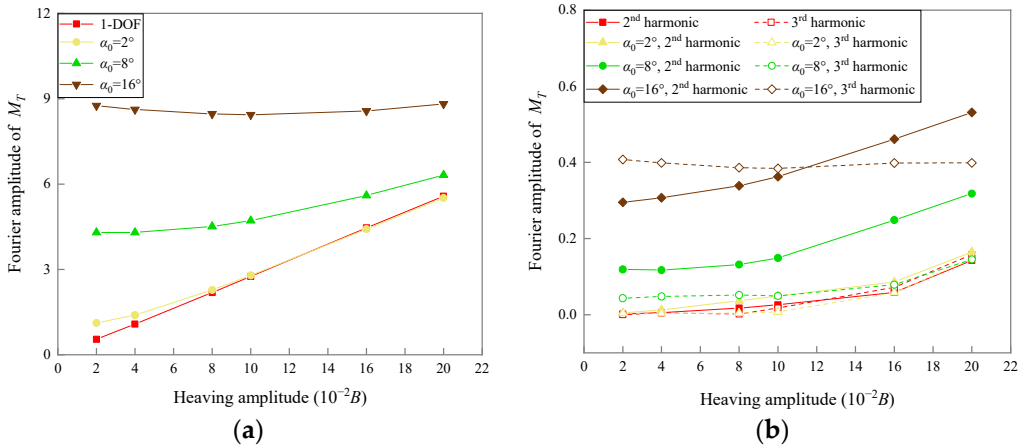

Figure 15. Variation in Fourier amplitude of aerodynamic moment with heaving amplitude. (**a**) The fundamental frequency; (**b**) Second harmonic and third harmonic.

As shown in Figures 16a and 17a, the linear relationship between fundamental frequency amplitude of aerodynamic forces and pitching amplitude involved is weak regardless of 1-DOF pitching motion or 2-DOF coupled motion, and the larger the amplitude, the weaker the linear characteristics. Therefore, pitching motion is considered to be the primary source form of nonlinear components. Figures 16b and 17b show that the curve shape of the second harmonic and third harmonic component with pitching amplitude is not significantly changed under different foundational heaving amplitudes, and both of

them show an increasing trend. With the increase in pitching amplitude, the growth rate of the third harmonic is higher than that of the second harmonic, and the growth range is significant under large amplitude. At this time, the importance of the third harmonic is prominent and should be paid attention to.

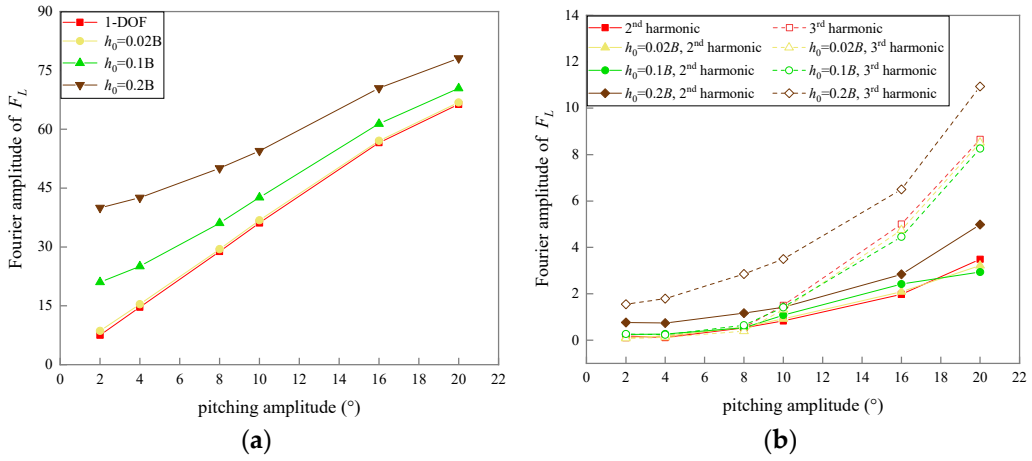

Figure 16. Variation in Fourier amplitude of aerodynamic lift with pitching amplitude. (**a**) The fundamental frequency; (**b**) Second harmonic and third harmonic.

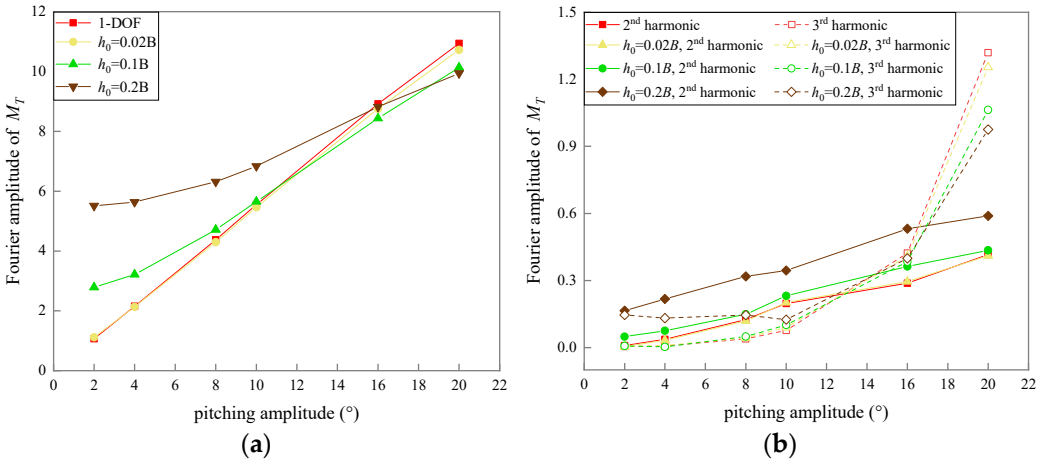

Figure 17. Variation in Fourier amplitude of aerodynamic moment with pitching amplitude. (**a**) The fundamental frequency; (**b**) Second harmonic and third harmonic.

In order to explore the law that the proportion of nonlinear aerodynamic components change with the coupled amplitude, the sum of the second to fifth harmonic components is used to represent the aerodynamic nonlinear components, and the total amount of the previous quintuple frequency is used as the cardinal number of normalized statistics, as shown in Figures 18–21.

Compared with the 1-DOF pitching motion, the proportion of nonlinear components of aerodynamic force is reduced due to the addition of a small amplitude heaving motion, as shown in Figures 18a and 19a. At this time, the heaving motion plays a positive damping role, and the positive damping action of the heaving motion decreases obviously with the increase in foundational pitching amplitude. For the aerodynamic lift, as shown in Figure 18b, the proportion of nonlinear components decreases first and then increases with heaving amplitude, and the heaving motion has an extreme value amplitude of positive damping action. For the aerodynamic moment, as shown in Figure 19b, the proportion of nonlinear components generally shows a positive correlation trend with increasing the heaving amplitude. In the 1-DOF pitching motion state, the proportion of

nonlinear components of aerodynamic lift is higher than that of aerodynamic moment, which has stronger nonlinear characteristics. However, due to the positive damping effect of small amplitude heaving motion, a slightly higher proportion of aerodynamic moment is observed near the extreme value amplitude of positive damping action. Therefore, the complex influence of a heaving motion amplitude on nonlinear characteristics should be considered when studying nonlinear flutter.

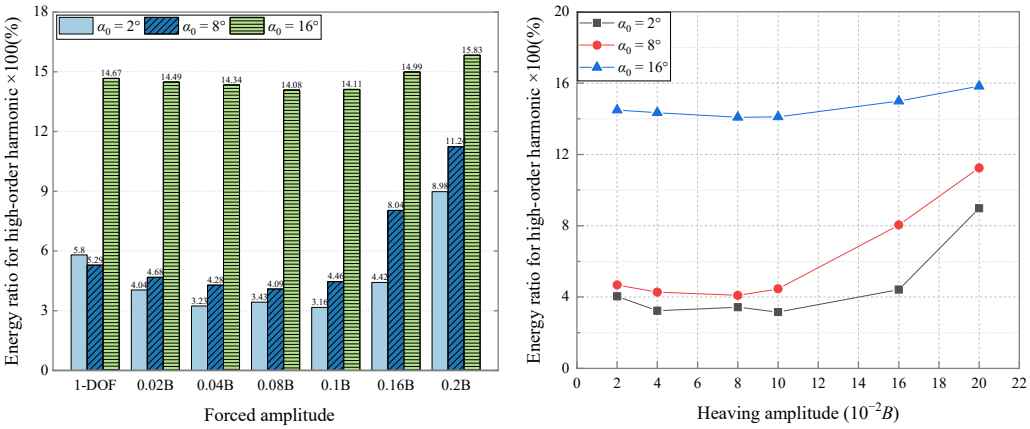

Figure 18. Proportion variation in high-order harmonic components of aerodynamic lift with different heaving amplitudes. (**a**) Comparison of 1-DOF pitching motion with 2-DOF coupled motion; (**b**) 2-DOF coupled motion.

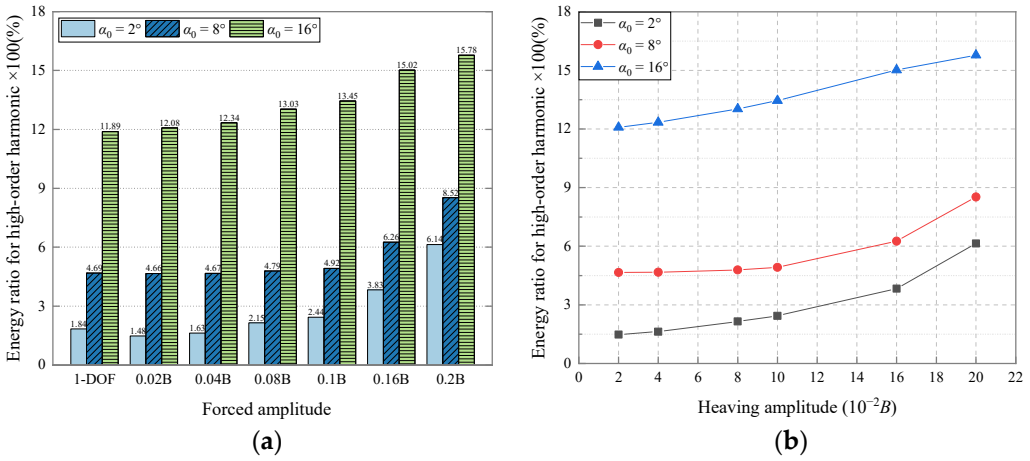

Figure 19. Proportion variation in high-order harmonic components of aerodynamic moment with different heaving amplitudes. (**a**) Comparison of 1-DOF pitching motion with 2-DOF coupled motion; (**b**) 2-DOF coupled motion.

Figures 20a and 21a show that compared with the 1-DOF heaving motion, the nonlinear components of aerodynamic moment increase with the addition of pitching motion, and the same results are also observed in the aerodynamic lift under the foundational heaving motion of small amplitude. The nonlinear aerodynamic components broadly positively correlated with the pitching amplitude, as reported in Figures 20b and 21b. Under different foundational heaving amplitudes, the difference in proportion of nonlinear components of aerodynamic forces (especially aerodynamic moment) decreases obviously with the increase in pitching amplitude. In conclusion, it is considered that the nonlinear components of aerodynamic forces in the coupled motion are mainly provided by pitching motion form, and the aerodynamic moment is more significantly affected by the pitching motion. In general, the proportion of nonlinear components of aerodynamic lift is higher than

that of aerodynamic moment, which has stronger nonlinear characteristics. Therefore, the nonlinear components of aerodynamic lift should be considered preferentially when optimizing the nonlinear model.

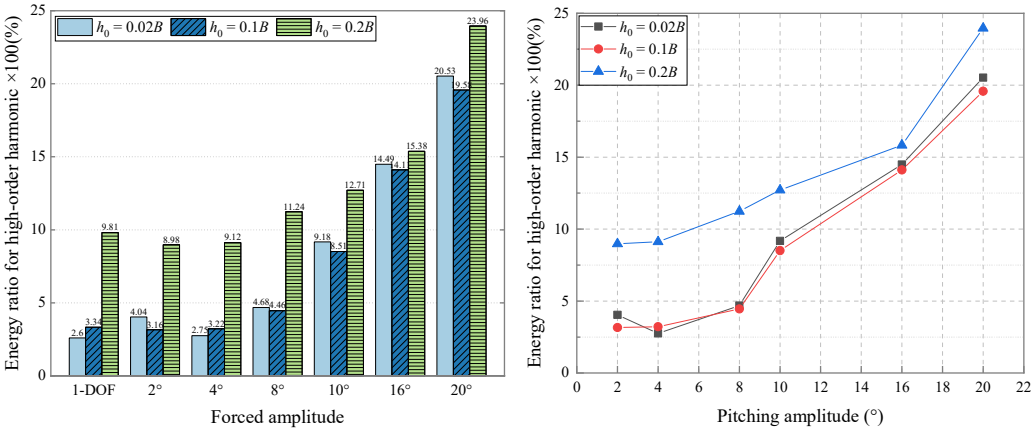

Figure 20. Proportion variation in high-order harmonic components of aerodynamic lift with different pitching amplitudes. (**a**) Comparison of 1-DOF heaving motion with 2-DOF coupled motion; (**b**) 2-DOF coupled motion.

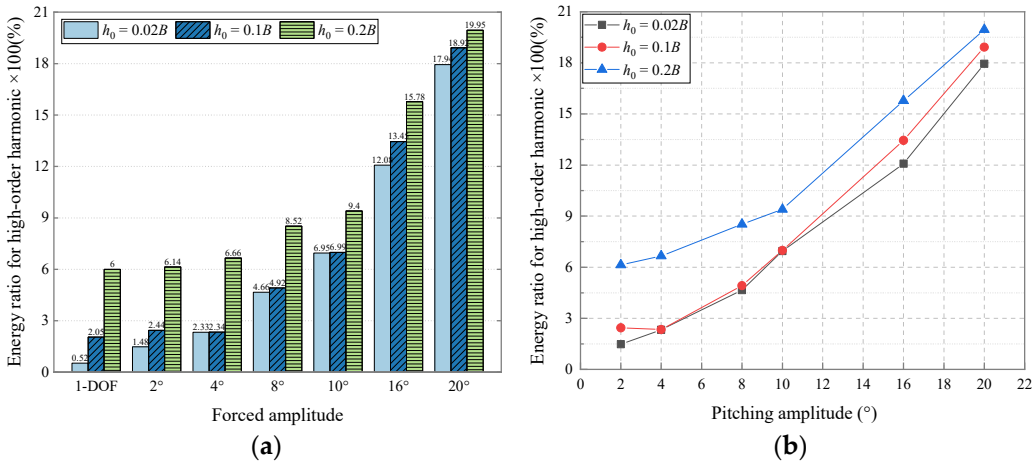

Figure 21. Proportion variation in high-order harmonic components of aerodynamic moment with different pitching amplitudes. (**a**) Comparison of the 1-DOF heaving motion with the 2-DOF coupled motion; (**b**) 2-DOF coupled motion.

In order to compare the variation characteristics of aerodynamic lift and moment with the coupling amplitude in detail, the proportion of nonlinear components in the 1-DOF motion of the section is taken as the cardinal number for normalized statistics, as shown in Figures 22 and 23.

Figure 22 shows that the positive damping action of small amplitude heaving motion in the aerodynamic lift is significantly stronger than that of aerodynamic moment. Figure 23 shows that the small amplitude pitching motion has a significantly stronger promoting effect on the nonlinear characteristics of aerodynamic moment than lift. Therefore, in the exploration of amplitude dependence of nonlinear components of the aerodynamic lift and moment under heaving-pitching coupled motion, it is found that the heaving motion mainly affects the nonlinear components of aerodynamic lift, while the pitching motion has a more significant effect on both, and has a stronger effect on aerodynamic moment. Although the nonlinear proportion of aerodynamic moment is generally lower than that of aerodynamic lift, its growth rate with amplitude is larger. Therefore, the nonlinear

component of aerodynamic moment should be attached to importance at large amplitudes, especially at large pitching amplitude.

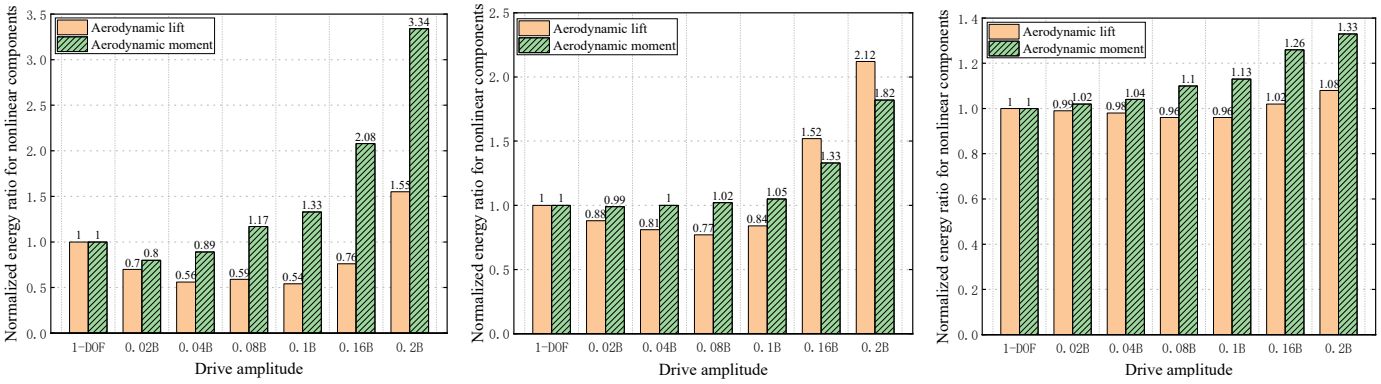

Figure 22. Normalized statistical diagram of aerodynamic nonlinear components in different heaving amplitude. (**a**) foundational pitching amplitude $\alpha_0 = 2°$; (**b**) foundational pitching amplitude $\alpha_0 = 8°$; (**c**) foundational pitching amplitude $\alpha_0 = 16°$.

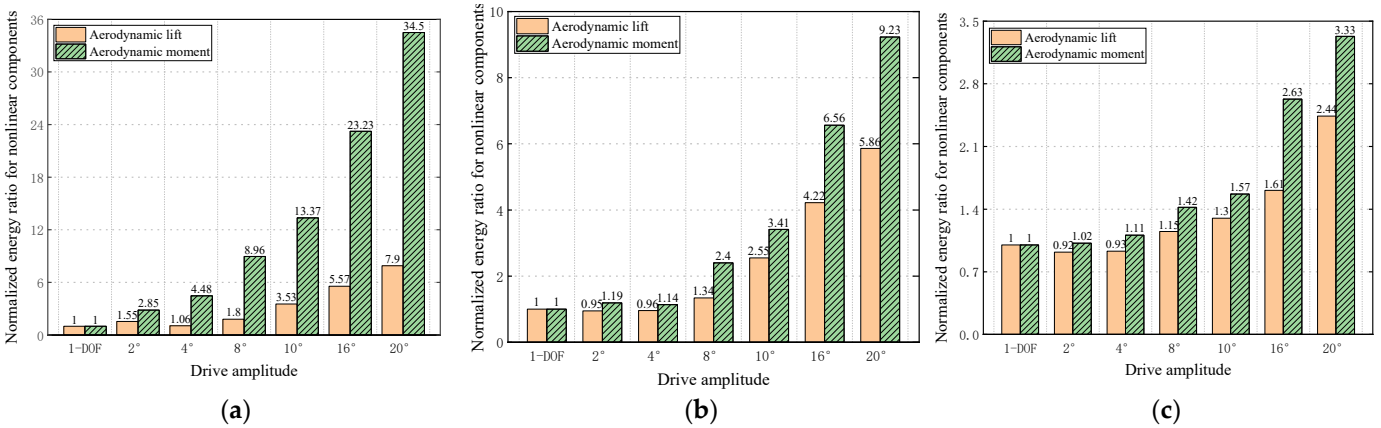

Figure 23. Normalized statistical diagram of aerodynamic nonlinear components in different pitching amplitude. (**a**) foundational heaving amplitude $h_0 = 0.02B$; (**b**) foundational heaving amplitude $h_0 = 0.1B$; (**c**) foundational heaving amplitude $h_0 = 0.2B$.

4. Conclusions

The amplitude dependence of nonlinear self-excited aerodynamic forces for the semi-closed box deck section under heaving-pitching coupled motion is investigated in this work. The combination form of forced amplitude is changed by dynamic grid technology, and the self-excited aerodynamic forces are obtained by forced vibration numerical simulation for discussion and analysis. Key conclusions deriving from the study include:

With the increasing pitching amplitude, the main components of the high-order harmonic of aerodynamic forces are transferred from the second harmonic to third in the heaving-pitching coupled motion. With the increasing heaving amplitude, the energy transfer phenomenon of aerodynamic lift is promoted, while that of aerodynamic moment is inhibited. Therefore, when the pitching amplitude is large ($\alpha_0 > 10°$), the importance of the third harmonic in the aerodynamic lift should be prioritized in nonlinear flutter calculation, while when the pitching amplitude is small ($\alpha_0 < 10°$), the importance of the second harmonic in the aerodynamic moment should be considered first.

Compared with the 1-DOF pitching motion, the proportion of nonlinear aerodynamic nonlinear component is reduced when the heaving motion of small amplitude is added. At this time, the small amplitude heaving motion plays a positive damping role in the coupled

motion. The heaving motion has little promoting effect on the aerodynamic nonlinear components, which mainly contributes to the aerodynamic lift, and has a complex influence on the nonlinear characteristics.

In the heaving-pitching coupled motion, the proportion of nonlinear components generally increases with the pitching amplitude, and the proportion of high-order harmonic components can reach more than 20% under large pitching amplitude ($\alpha_0 = 20^\circ$). The high harmonic components of aerodynamic forces are mainly generated by pitching motion, and the nonlinear characteristics of aerodynamic forces, especially aerodynamic moment, are mainly affected by pitching motion.

In general, the proportion of nonlinear components of aerodynamic lift is higher than that of aerodynamic moment, so more attention should be paid to the nonlinear research of aerodynamic lift. It is worth noting that the extreme value heaving amplitude of positive damping action is observed in the nonlinear aerodynamic lift, and the nonlinear component of aerodynamic moment has a higher growth rate with the increase in coupled amplitude. Therefore, the nonlinear research of aerodynamic moment should also be emphasized in the case of large amplitude and extreme value heaving amplitude.

Author Contributions: Conceptualization, H.L. and J.J.; methodology, H.L.; software, H.L.; validation, H.L., J.J. and L.Z.; formal analysis, H.L. and J.J.; investigation, H.L. and L.D.; resources, J.J.; data curation, H.L.; writing—original draft preparation, H.L.; writing—review and editing, H.L.; visualization, H.L.; supervision, J.J.; project administration, J.J.; funding acquisition, J.J. All authors have read and agreed to the published version of the manuscript.

Funding: This study was financially supported by NSFC under grant No. 51908108.

Conflicts of Interest: The authors declare no conflict of interest.

References

1. Diana, G.; Fiammenghi, G.; Belloli, M.; Rocchi, D. Wind tunnel tests and numerical approach for long span bridges: The Messina bridge. *J. Wind Eng. Ind. Aerodyn.* **2013**, *122*, 38–49. [CrossRef]
2. Mannini, C.; Sbragi, G.; Schewe, G. Analysis of self-excited forces for a box-girder bridge deck through unsteady RANS simulations. *J. Fluids Struct.* **2016**, *63*, 57–76. [CrossRef]
3. Daito, Y.; Matsumoto, M.; Araki, K. Torsional flutter mechanism of two-edge girders for long-span cable-stayed bridge. *J. Wind Eng. Ind. Aerodyn.* **2002**, *90*, 2127–2141. [CrossRef]
4. Lin, S.; Wang, Q.; Nikitas, N.; Liao, H. Effects of oscillation amplitude on motion-induced forces for 5: 1 rectangular cylinders. *J. Wind Eng. Ind. Aerodyn.* **2019**, *186*, 68–83. [CrossRef]
5. Zhang, Z.T.; Wang, Z.X.; Zeng, J.D.; Zhu, L.D.; Ge, Y.J. Experimental investigation of post-flutter properties of a suspension bridge with a p-shaped deck section. *J. Fluids Struct.* **2022**, *112*, 103592. [CrossRef]
6. Noda, M.; Utsunomiya, H.; Nagao, F.; Kanda, M.; Shiraishi, N. Effects of oscillation amplitude on aerodynamic derivatives. *J. Wind Eng. Ind. Aerodyn.* **2003**, *91*, 101–111. [CrossRef]
7. Scanlan, R.H.; Tomko, J.J. Airfoil and Bridge Deck Flutter Derivatives. *J. Eng. Mech. Div.* **1971**, *97*, 1717–1737. [CrossRef]
8. Diana, G.; Resta, F.; Rocchi, D. A new numerical approach to reproduce bridge aerodynamic non-linearities in time domain. *J. Wind Eng. Ind. Aerodyn.* **2008**, *96*, 1871–1884. [CrossRef]
9. Diana, G.; Resta, F.; Zasso, A.; Belloli, M.; Rocchi, D. Forced motion and free motion aeroelastic tests on a new concept dynamometric section model of the Messina suspension bridge. *J. Wind Eng. Ind. Aerodyn.* **2004**, *92*, 441–462. [CrossRef]
10. Kral, R.; Pospisil, S.; Naprstek, J. Wind tunnel experiments on unstable self-excited vibration of sectional girders. *J. Fluids Struct.* **2014**, *44*, 235–250. [CrossRef]
11. Náprstek, J.; Pospíšil, S.; Hračov, S. Analytical and experimental modelling of non-linear aeroelastic effects on prismatic bodies. *J. Wind Eng. Ind. Aerodyn.* **2007**, *95*, 1315–1328. [CrossRef]
12. Amandolese, X.; Michelin, S.; Choquel, M. Low speed flutter and limit cycle oscillations of a two-degree-of-freedom flat plate in a wind tunnel. *J. Fluids Struct.* **2013**, *43*, 244–255. [CrossRef]
13. Li, W.; Laima, S. Experimental Investigations on Nonlinear Flutter Behaviors of a Bridge Deck with Different Leading and Trailing Edges. *Appl. Sci.* **2020**, *10*, 7781. [CrossRef]
14. Arena, A.; Lacarbonara, W.; Marzocca, P. Post-Critical Behavior of Suspension Bridges Under Nonlinear Aerodynamic Loading. *J. Comput. Nonlinear Dyn.* **2016**, *11*, 11005. [CrossRef]
15. Matsumoto, M.; Daito, Y.; Yoshizumi, F.; Ichikawa, Y.; Yabutani, T. Torsional flutter of bluff bodies. *J. Wind Eng. Ind. Aerodyn.* **1997**, *69*, 871–882. [CrossRef]

16. Xu, F.Y.; Yang, J.; Zhang, M.J.; Yu, H.Y. Experimental investigations on post-flutter performance of a bridge deck sectional model using a novel testing device. *J. Wind Eng. Ind. Aerodyn.* **2021**, *217*, 104752. [CrossRef]
17. van Rooij, A.; Nitzsche, J.; Dwight, R.P. Energy budget analysis of aeroelastic limit-cycle oscillations. *J. Fluids Struct.* **2017**, *69*, 174–186. [CrossRef]
18. Larsen, A. Advances in aeroelastic analyses of suspension and cable-stayed bridges. *J. Wind Eng. Ind. Aerodyn.* **1998**, *74*, 73–90. [CrossRef]
19. Zhu, J.; Zheng, S.; Tang, Y.; Guo, J. A study on the nonlinear flutter amplitude characteristics of a streamlined box girder section. *J. Sound Vib.* **2018**, *37*, 158–165.
20. Huang, L.; Liao, H. Nonlinear aerodynamic forces on the flat plate in large amplitude oscillation. *Int. J. Appl. Mech.* **2013**, *5*, 554–563. [CrossRef]
21. Zhang, Z.; Zhang, X.; Yang, Y.; Ge, Y. Nonlinear aerodynamic and energy input properties of a twin-box girder bridge deck section. *J. Fluids Struct.* **2017**, *74*, 413–426. [CrossRef]
22. Jia, J.; Lu, H.Y.; Li, X.B.; Chen, Q. Study on Aerodynamic Nonlinear Characteristics of Semiclosed Box Deck Based on Variation of Motion Parameters. *Adv. Civ. Eng.* **2022**, *2022*, 4711844. [CrossRef]
23. Zhang, M.J.; Xu, F.Y.; Zhang, Z.B.; Ying, X.Y. Energy budget analysis and engineering modeling of post-flutter limit cycle oscillation of a bridge deck. *J. Wind Eng. Ind. Aerodyn.* **2019**, *188*, 410–420. [CrossRef]
24. Zhu, L.; Gao, G. Influential factors of soft flutter phenomenon for typical bridge deck sections. *J. Tongji Univ.* **2015**, *43*, 1289–1294, 1382.
25. Zhu, L.-D.; Gao, G.-Z.; Zhu, Q. Recent advances, future application and challenges in nonlinear flutter theory of long span bridges. *J. Wind Eng. Ind. Aerodyn.* **2020**, *206*, 104307. [CrossRef]
26. Boussinesq, M.J. Essai sur la théorie des eaux couarantes. *Mémories Préséents Par Divers. Savants L'académie Des Sci.* **1877**, *23*, 678–680.
27. Menter, F.R. Two-equation eddy-viscosity turbulence models for engineering applications. *Aiaa J.* **1994**, *32*, 1598–1605. [CrossRef]
28. Wu, T.; Kareem, A. Modeling hysteretic nonlinear behavior of bridge aerodynamics via cellular automata nested neural network. *J. Wind Eng. Ind. Aerodyn.* **2011**, *99*, 378–388. [CrossRef]
29. Wu, T.; Kareem, A. A nonlinear analysis framework for bluff-body aerodynamics: A Volterra representation of the solution of Navier-Stokes equations. *J. Fluids Struct.* **2015**, *54*, 479–502. [CrossRef]
30. Wang, S.; Ingham, D.B.; Ma, L.; Pourkashanian, M.; Tao, Z. Turbulence modeling of deep dynamic stall at relatively low Reynolds number. *J. Fluids Struct.* **2012**, *33*, 191–209. [CrossRef]
31. Zanotti, A.; Nilifard, R.; Gibertini, G.; Guardone, A.; Quaranta, G. Assessment of 2D/3D numerical modeling for deep dynamic stall experiments. *J. Fluids Struct.* **2014**, *51*, 97–115. [CrossRef]
32. Liaw, K. Simulation of Flow around Bluff Bodies and Bridge Deck Sections Using CFD. Ph.D. Theses, University of Nottingham, Nottingham, UK, 2005.